Evidence of Piezoelectric Potential and Screening Effect in Single Highly Doped ZnO:Ga and ZnO:Al Nanowires by Advanced Scanning Probe Microscopy

Oleksandr Synhaivskyi, David Albertini, Pierre Gaffuri, Jean-Michel Chauveau, Vincent Consonni, Brice Gautier, Georges Bremond

Evidence of Piezoelectric Potential and Screening Effect in Single Highly Doped ZnO:Ga and ZnO:Al Nanowires by Advanced Scanning Probe Microscopy

Oleksandr Synhaivskyi[1], David Albertini[2], Pierre Gaffuri[3,4], Jean-Michel Chauveau[5], Vincent Consonni[3], Brice Gautier[2], Georges Bremond[2]*

[1]Université de Lyon, Institut des Nanotechnologies de Lyon, UMR 5270 CNRS, Ecole Centrale de Lyon, 36 avenue Guy de Collongue, 69134 Ecully cedex, France
[2]Université de Lyon, Institut des Nanotechnologies de Lyon, UMR 5270 CNRS, INSA de Lyon, 7 avenue Jean Capelle, 69621 Villeurbanne cedex, France
[3]Univ. Grenoble Alpes, CNRS, Grenoble INP, LMGP, F-38000 Grenoble, France;
[4]Univ. Grenoble Alpes, CNRS, Grenoble INP, Institut Néel, F-38000 Grenoble, France
[5]Université Côte d'Azur, CNRS, CRHEA, Rue B. Gregory, 06905 Sophia Antipolis Cedex, France

***Corresponding Author:**

Oleksandr Synhaivskyi

Université de Lyon, Institut des Nanotechnologies de Lyon, UMR 5270 CNRS, Ecole Centrale de Lyon, 36 avenue Guy de Collongue, 69134 Ecully cedex, France

oleksandr.synhaivskyi@ec-lyon.fr

Abstract

A complete study based on advanced atomic force microscopy (AFM) electrical mode called scanning spreading resistance microscopy (SSRM) is carried out on a series of samples of zinc oxide (ZnO) nanowires grown by chemical bath deposition (CBD) with different doping concentrations using gallium (Ga). The concentration of free charge carriers determined through SSRM signal calibration with a specific molecular beam epitaxy (MBE) grown multilayer structure with variation in each layer of electrically active Ga doping ranges from 1×10^{17} to 7×10^{20} at/cm^3. The concentration of free charge carriers found changes in every nanowire sample with a different ratio of the doping precursor. It increases from 3×10^{18} at/cm^3 in non-intentionally doped (NiD) nanowires to 7.6×10^{19} at/cm^3 in samples grown with a doping precursor concentration $[Ga(NO_3)_3]/[Zn(NO_3)_2]$ of more than 2%, which makes it possible to gradually dope the nanowires with more accurate regulation of the precursor concentration. A similar electrical activity for aluminum (Al) doped nanowires is found. Piezoresponse force microscopy (PFM) in dual-frequency resonance tracking (DFRT) mode reveals a stable piezoelectric activity of highly doped nanowires that is presumably attributed to the increased surface trap density causing a Fermi level pinning when ZnO nanowires are grown at a high pH value favorable for the intentional doping. It also shows the degradation of piezoelectric properties caused by the "screening effect," which directly correlates with the increase of free charge carrier concentration in nanowires. PFM in DFRT mode is eventually proposed as an original direct method for analyzing the electrical properties of a single piezoelectric nanowire.

KEYWORDS: ZnO, nanowires, free charge carrier concentration, NW polarity, screening effect, calibrated spreading resistance microscopy, piezoresponse force microscopy

Introduction

Zinc Oxide (ZnO) has great potential for applications in electronics and optoelectronics due to its outstanding properties such as a wide bandgap energy around 3.37 eV at

room temperature, a considerable excitation binding energy of 60 meV at room temperature, and low power threshold for optical pumping[1]. The recent studies have shown the effectiveness of the use of ZnO nanostructures including high aspect ratio nanowires in various applications where the optical[2], electrical[3,4], and piezoelectric[5,6] properties of the material play a major role. In the field of piezoelectricity, one of the major effects originates from the significant increase in piezoelectric constants as the size of nanowires is decreased along with the beneficial role of surfaces, which can be potentially used for effective energy harvesting and pressure sensing devices.[7,8] The basic principle of operation of vertically integrated nanogenerators (VING) is related to a combination of piezoelectric and semiconductor properties for charge creation, accumulation, and discharge process voltage drop created across the cross-section of the NW when it is laterally deflected[9], or compressed[10] with the tensile side surface in positive voltage and compressive side in a negative voltage. In that configuration, it is crucial to quantitatively determine the voltage at the two side surfaces of the nanowire for finding the best efficiency of the piezoelectric nanogenerator and the operation voltage of the nano-piezotronics. Therefore, for the output parameters of the device, it is necessary to control all factors that affect piezoelectric properties, which includes geometric parameters of the nanowires, nanowire density, and polarity orientation. Also, the high free charge carrier concentration, which is usually found in nanowires grown by different methods[11,12], represents the main challenge for improving the performances of pressure sensors and nanogenerators. The principle of operation of a nanogenerator creates a periodic piezoelectric potential during periodic deformation, which moves the electrons in the external circuit to balance the Fermi level; however, free charge carriers also migrate and partially reduce this potential[13]. Most commonly, this effect is called “screening effect” and it has been proved to severely limit the output voltage of the piezoelectric devices[10,14]. The effect of resistivity on piezoelectric was demonstrated by Scrymgeour et al.[15], however, the influence of the polarity was not taken into account as well as the estimation of free charge carriers were in the very wide range to prove the screening effect. Moreover, measurement of piezoelectric response at frequencies outside

resonance may not be sensitive enough to determine the piezoelectricity of a highly dopped materials. Due to the complexity of decoupling the different geometrical contributions, the evolution of the piezoelectric potential as a function of the free charge carrier concentration has not been experimentally revealed yet. On the other hand, highly doped ZnO nanowires are considered as promising for transparent electronics thanks to its good light transmittance, metallic-like conductivity, and good adhesion to the flexible substrates[16]. The other advantages of ZnO nanowires also include chemical inertness and biocompatibility[17].

Eventually, the control of free charge carrier concentration in ZnO nanowires remains a challenging task due to its small size and to the inherent difficulty to implement the intentional doping in numerous growth methods including wet chemistry. In that respect, the widely-used chemical bath deposition as a versatile, low-temperature growth method that is compatible with the fabrication of flexible piezoelectric devices can form vertically aligned ZnO nanowires with a dedicated morphology on a large number of substrates using spontaneous or selective area growth approaches[18]. However, the development of their intentional doping in aqueous solution is still a huge issue. Recently, a couple of investigations have shown that attractive electrostatic interactions involving dopant ion complexes with the charged *m*-plane sidewalls of ZnO nanowires result in the monitoring of their aspect ratio[19] and in the introduction of dopants in the center of ZnO nanowires,[20,21] opening the way for tuning their free charge carrier concentration. The possibility to control the dopant concentration such as Al and Ga in ZnO nanowires grown by chemical bath deposition further requires a very careful control of the conditions in the bath like pH[20,21]. The determination of the free charge carrier concentration in ZnO nanowires is also one of the essential tasks in developing a real device manufacturing technology. Two well-known methods for obtaining reliable information on the resistivity and mobility of ZnO nanowires have relied on the 4-point probe Van-der-Pauw measurement[22] and the field effect transistor (FET) structure,[3,23] but, due to the nanometric size of the nanowire, it requires complex sample technology preparation, and its spatial resolution is limited owing to the need for controlling the position of the probes[24].

More practical approaches for the determination of the free charge carrier concentration in semiconductors at the nanoscale level are based on atomic force microscopy (AFM) measurements in scanning capacitance microscopy (SCM) mode. The method is based on a change in electrostatic capacitance between the surface and the probe, which can provide a full 2D map of charge carriers near the surface of the sample. In the case of the characterization of ZnO nanowires, the sample-tip system in the ambient environment acts as a metal-oxide-semiconductor (MOS) structure, but the nature of this structure is not fully understood[25]. Furthermore, getting consistent and repeatable results for highly conductive materials remains challenging. The SCM measurement results for the calibration sample (Figure S4) and the non-dopped nanowires sample (Figure S5) discussed in this article are given in the supporting information. The other mode called scanning spreading resistance microscopy (SSRM) could be a better-adapted alternative tool for the electrical characterization of nanostructures with resolution down to 10 nm in the air[26] and 1 nm in vacuum[27]. Indeed, the repeatability of SSRM measurements in ZnO under ambient conditions is higher than the SCM measurements due to uncontrollable thickness of water layer which acts as dielectric. SSRM is a direct current-based measurement method that uses logarithmic amplification to measure the volume spreading resistance of the sample in the wide range between 10^4 and 10^{10} Ohm. Its further combination with piezoelectric force microscopy (PFM) measurements is expected to yield a direct comparison of the electrical and piezoelectric properties at the nanoscale, leading to a better understanding of the piezoelectric potential screening. However, this combination has never been reported so far. It can also serve as a method of quality control of the base element of a nanowire-based device.

In this article, ZnO nanowires are grown by chemical bath deposition with different ratios of the doping precursor, the same annealing temperature, and the same pH of the growth environment with the aim of gradual control of the free charge carrier concentration. They are analyzed with the SSRM electrical mode and piezoresponse force microscopy in dual frequency

resonance tracking mode (PFM DFRT) after a dip-coating encapsulation and chemo-mechanical planarization process.

Results

Morphology of Al- and Ga-doped ZnO nanowires

The growth of intentionally doped ZnO nanowires was achieved by chemical bath deposition on a polycrystalline ZnO seed layer deposited by dip coating on silicon[28]. The same conditions using $Zn(NO_3)_2$ and HMTA at an equimolar concentration of 30 mM and a growth temperature of 85 °C were used along with the addition of ammonia to control the initial pH at a value of 10.9 and of $Al(NO_3)_3$ and $Ga(NO_3)_3$ to achieve an intentional doping.[20,21].The SSRM measurements require contact with a significant downforce between the nanowire and the AFM tip. As-grown ZnO nanowires are not suitable for such measurements because of the large space gap between them, as revealed in Figure 1(a). In this case, it is necessary to consolidate the nanowires by filling this space with a solid insulating matrix followed by polishing to create a low roughness 2D surface of the matrix and nanowires on the sample,[29,30] as shown in Figure 1(b). Thus, a surface with root-mean-square (RMS) roughness less than 3 nm was reached, while the tops of the nanowires are extended from the dielectric matrix from 5 to 15 nm, thereby making it possible to obtain a stable electric contact between the nanowires and the AFM conductive tip through the substrate.

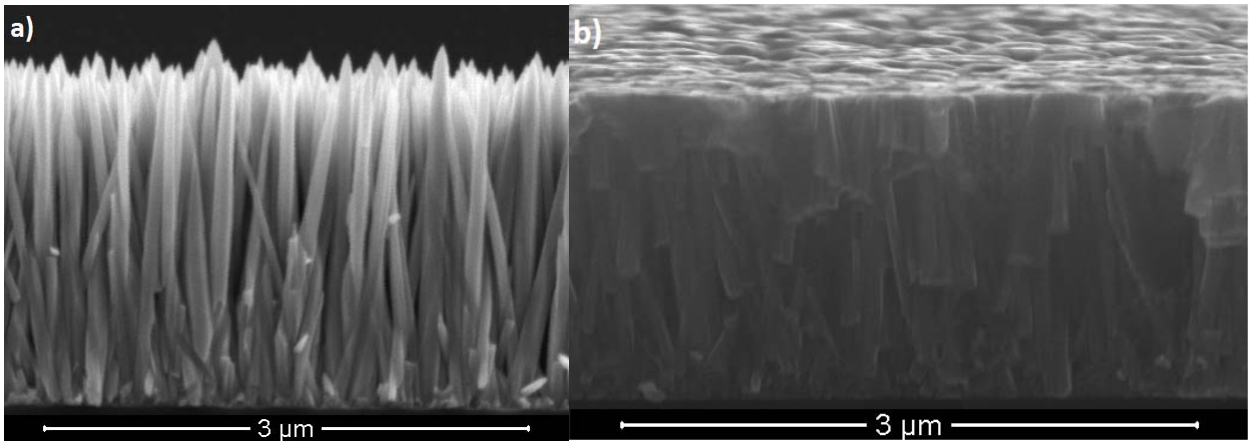

Figure 1. a) Cross-sectional (90º) field emission scanning electron microscopy (FESEM) image of 2.5% Ga doped nanowires after CBD deposition b) Tilted cross-sectional (84º) FESEM image of 2.5% Ga doped nanowires after encapsulation in SiO_2 matrix and chemo-mechanical polishing with the average RMS roughness of 3.2 nm

Electrical Properties of Al- and Ga-doped ZnO nanowires

The interpretation of the measured SSRM resistance takes its roots from spreading resistance profiling and is defined as the ratio of the resistivity of the sample to the contact radius[31]. $R = CF(a,\rho)\frac{\rho}{2a} + R_{barrier}(\rho) + R_{tip} + R_{bulk}$, where a is the contact radius assumed to be circular, $CF(\rho, a)$ is the correction factor as a function of the 3-dimensional profile of the resistivity, $R_{barrier}$ is the component of the measured resistance related to the interface between the sample and the AFM tip. This formula is valid only for the case when spreading resistance dominates over ballistic resistance where the free mean path of the electrons λ is much smaller than the contact radius a. Otherwise, the measured spreading resistance is described by the Sharvin Resistance $R_{Sharvin} = \frac{4\rho\lambda}{3\pi a^2}$ [32]. However, the exact value is neither known for the free path of electrons λ nor for the electrically effective radius a. A more practical approach for establishing the concentration of free charge carriers as the most impactful parameter in the conductivity of nanowires is thus based on the calibration method[33]. With the help of specially prepared multilayer samples with a known concentration of free charge carriers, it is possible to quantitatively establish the unknown concentration of free charge carriers in a single nanowire, avoiding an unknown parameter as an electrically effective radius and minimizing errors of a change in mobility.

For this study, a sample was grown by molecular beam epitaxy (MBE) on a ZnO single crystal with 18 layers exhibiting a thickness from 60 to 80 nm with a variation of gallium content. Secondary ion mass spectroscopy (SIMS) measurements quantitatively show the doping concentration of Ga for each layer; the amount of gallium ranges from 4×10^{17} to 5×10^{20} at/cm^3 in between layers with non-intentionally doped regions. For AFM measurements, the sample was

cleaved and placed on a vertical sample holder. For contact, a silver epoxy was applied to the top of the sample with a connection to the conductive part of the holder. The measurements were carried out as close as possible to the area with silver epoxy to eliminate material bulk resistance. In this configuration, the current lines do not cross other layers, and the system has the greatest resemblance to measurements on nanowires. All measurements were performed on the same day with the same tip, with the same applied force, with the same scanning speed in order to eliminate the impact of the number of factors related to experiment configuration such as the difference of tip shape, the laser position on the cantilever, the applied force. Figure 2(a) shows the results of the SSRM measurement image and its comparison with SIMS profile. In MBE grown ZnO thin films, the near-unity activation of the Ga dopant has been reported for the doped range between 10^{18} and $10^{20}cm^{-3}$ [34]. Assuming that the concentration of free charge carriers in the calibration sample is equal to the Ga concentration, a relation between the measured SSRM resistance and the concentration of free charge carriers can be established. Thus, by measuring the SSRM on planarized nanowires and comparing the signals received from the multilayer structure Figure 2(b), it becomes possible to determine the concentration of free charge carriers in a single nanowire with a good accuracy.

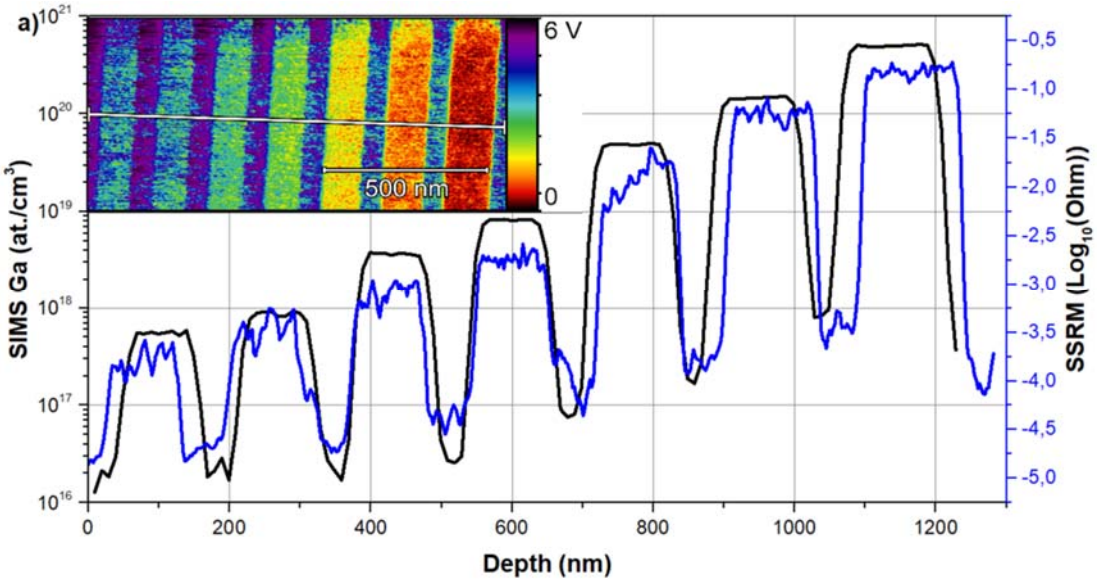

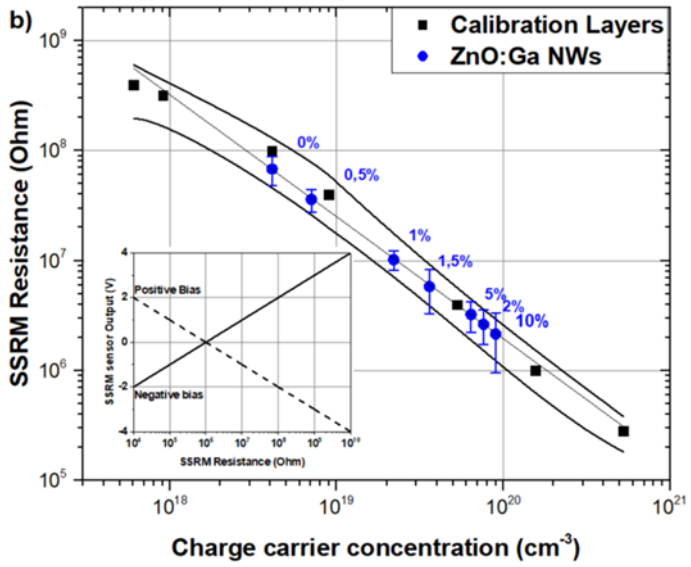

Figure 2. a) SIMS doping profile of seven ZnO: Ga layers doped from 6×10^{18} to 7×10^{20} cm^{-3} compared to SSRM data profile captured from the cleaved area. b) Calibration curve with data obtained from nanowires. Error bars represent the statistical error. The inserted small graph shows the correlation between raw SSRM data measured in (V) and total measured stack resistance (Ohm).

Typically obtained images of topography and SSRM resistance data are shown in Figure 3. No correlation with the topography on the nanowire was observed in the measured signal. Also, within the same image, the difference between the signals from nanowires of different diameters is insignificant. The distribution of free charge carriers is thus uniform and constant and does not depend on the nanowire diameter. To minimize the error of spreading resistance, nanowires with the same cross-sectional area exhibiting a diameter of 80 ± 10 nm were chosen for analysis.

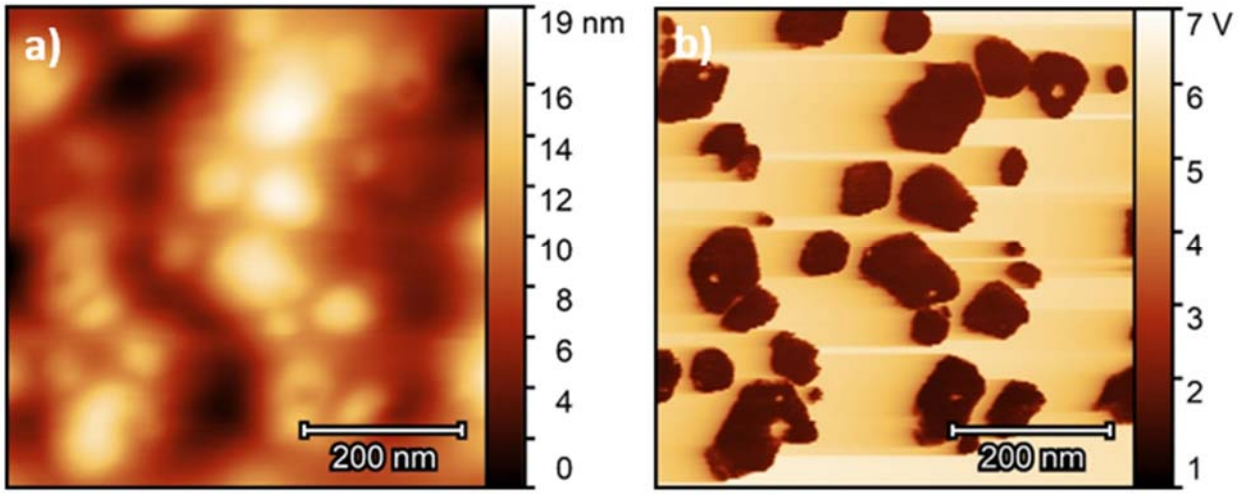

Figure 3. a) Topography of NiD nanowires sample after encapsulation into the dielectric matrix and chemo-mechanical polishing. Captured in contact mode b) SSRM resistance profile obtained on NiD ZnO encapsulated nanowires. Scan size – 600 x 600 nm (F_{app} = 2.4 μN, V_{bias} = 2V, $k_{CDT-NCHR}$ = 67.20 N/m). The examples of images for the whole series of samples are given in supporting information (Figure S1).

From each sample, a minimum of twenty SSRM profiles was collected from different nanowires and averaged. From the calibration curve in Figure 2(a), the concentrations of free charge carriers in nanowires were determined and represented in Figure 2 (b). The result of the characterization is shown in Table 1. When calculating the errors, only the statistical measurement error was taken into account from a same day experiment. All deviations represent a statistical error from various uncontrolled factors during the different experiments and do not exceed third an order of magnitude from the values as indicated in Table 1.

$[Ga(NO_3)_3]/[Zn(NO_3)_2]$	SSRM Resistance (Ohm)	Charge carrier Concentration (cm^{-3})	Estimated Resistivity (mΩ×cm)
0%	6.80×10^{7}	$3{,}10\times10^{18}$	25,16 – 40,26
0,5%	3.60×10^{7}	$7{,}05\times10^{18}$	11,06 – 17,70
1%	1.02×10^{7}	$2{,}20\times10^{19}$	3,54 – 5,67
1,5%	5.80×10^{6}	$3{,}60\times10^{19}$	2,16 – 3,46
2,5%	2.64×10^{6}	$7{,}60\times10^{19}$	1,02 – 1,64
5%	3.24×10^{6}	$6{,}40\times10^{19}$	1,21 – 1,95
10%	2.15×10^{6}	$9{,}00\times10^{19}$	0,86 – 1,38

Table 1. Electrical properties of Ga doped ZnO nanowires.

The high concentration of free charge carriers around 3.10 x 10^{18} cm^{-3} in unintentionally doped ZnO nanowires is attributed to the presence of a large number of hydrogen-related defects, namely interstitial hydrogen in bond centered sites (H_{BC}), substitutional hydrogen on the oxygen lattice sites (H_O), and zinc vacancy - hydrogen complexes (V_{Zn}-*n*H), all of them acting as shallow donors[12,35]. Accordingly, most of the ZnO nanowires exhibit a metallic-type bulk conduction by exceeding the effective critical concentration of 4.2 x 10^{18} cm^{-3} corresponding to the Mott transition[36]. The introduction of $Ga(NO_3)_3$ in the chemical bath with a concentration ratio up to 2 % has a significant effect on the concentration of free charge carriers increasing up to 7.6 x 10^{19} cm^{-3}, thereby making it possible to gradually control the intentional doping in ZnO NWs grown by chemical bath deposition. It is believed that a high density of substitutional Ga on the zinc lattice sites (Ga_{Zn}) acting as shallow donors with a low formation energy is induced here, along with the formation of zinc vacancy – Ga_{Zn} complexes (V_{Zn}-Ga_{Zn}) as a deep acceptor[37] following the thermal treatment during the sample preparation. It is further worth noticing that interstitial Ga with a much larger formation energy is not supposed to be formed. The maximum concentration of free charge carriers of 9 x 10^{19} cm^{-3} was found for a $Ga(NO_3)_3$ concentration ratio of 10 %. The present value is fairly close to the maximum concentration of free charge carriers induced by the Ga doping in ZnO thin films (i.e. 4.2×10^{20})[38]. Starting from a $Ga(NO_3)_3$ concentration ratio of 2 %, no significant change in the concentration of free charge carriers was thus shown. By adding a larger amount of $Ga(NO_3)_3$ during the growth by chemical bath deposition, it is possible to control the morphology of ZnO nanowires without drastically changing their electrical properties. It is not possible to directly establish the exact values of the resistivity using the ballistic conduction theory of SSRM since it is impossible to measure the exact radius of the electrically effective contact between the tip and the nanowire, just as we do not have sufficient information about mobility in nanowires. Although studies of the doped nanowire by STEM-EDS indicate that the distribution of Ga is uniform throughout the nanowire[21], which

allows the parameters associated with the uneven distribution of free charge carrier concentration to be ignored, the exact value of the resistivity in nanowires requires knowledge of many other parameters, which includes the contact radius, the mean free path of electrons as a function of the concentration of free charge carriers λ(n), the contact barrier resistance as a function of resistivity $R_{barrier}(\rho)$. However, it is possible to evaluate the change in resistivity. The value of mobility has been reported from FET measurements to lie in the range of 50-80 $cm^2/V\times s$[23,39]. Based on the values and from the equation of resistivity $\rho = 1/qn\mu_n$, the range of resistivity in ZnO nanowires was determined and reported in Table 1. A significant drop in their resistivity from (25.16 - 40.26) mΩ×cm for unintentionally doped nanowires to (0.86 - 1.38) mΩ×cm for Ga-doped nanowires is revealed, which is in good agreement with the four-point probe resistivity method carried out on almost similar nanowires[12,35]. In the case of Al doping, its incorporation mechanism is pretty similar to the incorporation mechanism of Ga as both elements belong to the same III column. However, since the ionic radius of Ga^{3+} is closer to the one of Zn^{2+} than to the one of Al^{3+} [40], it can lead to the fact that the conductivity of nanowires doped with Al can be less than the one of nanowires doped with Ga. Al-doped nanowires were grown by the same method and with the same growth parameters as Ga-doped nanowires with the only difference that $Al(NO_3)_3$ was used instead of $Ga(NO_3)_3$ [20]. In this study, three samples with a doping precursor concentration of 1%, 5%, and 7% were analyzed. The measurement results are shown in Table 2. Despite the predictions, all three samples of the SSRM resistance were found at the same level as Ga-doped nanowires starting from a precursor concentration of more than 1%.

$[Al(NO_3)_3]/[Zn(NO_3)_2]$	SSRM Resistance (Ohm)	Charge carrier Concentration (cm^{-3})	Estimated Resistivity (mΩ×cm)
1%	1.29×10^6	$1{,}09\times10^{20}$	0,07 – 1,15
5%	1.02×10^7	$2{,}20\times10^{19}$	3,55 – 5,67
7%	2.70×10^7	$3{,}90\times10^{19}$	2,00 – 3,20

Table 2. Electrical properties of ZnO: Al Nanowires

The same SSRM raw signal corresponds to the same product between the mobility and concentration of free charge carriers. From the present experiments, we can assume to a first approximation that mobility does not change much in Al- and Ga-doped nanowires. Then the concentration of free charge carriers can be derived from the calibration sample doped with Ga. The maximum concentration of free charge carriers was found to be 1.09×10^{20} cm^{-3}. This is half an order of magnitude less than that found in Al-doped ZnO thin films (i.e. 5.0×10^{20})[40]. In the absence of any data regarding the mobility change, the free charge carrier concentration from Table 2 remains a rough estimation. The AFM images for ZnO: Al series of samples are given in supporting information (Figure S3).

Influence of Free Charge Carrier Concentration on the Piezoelectric Properties of Al- and Ga- doped ZnO Nanowires

In general, PFM represents one of the known methods used for piezoelectric and ferroelectric characterization of nanostructures and is based on the inverse piezoelectric effect[41–44]. Putting the tip in contact with the top of the nanowire and applying AC bias makes it vibrate. The piezoelectric motion could be registered by the vertical and/or lateral displacement of the tip. In the simplified case, the coupling of electric potential with mechanical vibration is described by piezoelectric coefficients and described by formula $d_{33} = \Delta x_s/E_s$., if the electric field E_s and mechanical displacement Δx_s directed along the axis of polarization. Applying the PFM technique to measure the properties of piezoelectric II-VI and III-V semiconductors can be challenging, considering the fact that its piezoelectric constants (1-25 pm/V) are significantly lower than some ferroelectric materials (100-2000 pm/V)[45,46]. However, amplification of the response signal is possible with the measurements close to contact resonance between the sample and the tip, the frequency of which is approximately four times higher than the free resonance of the cantilever[47]. To compare vibration amplitudes, it is necessary to take into account changes in the contact resonance frequency due to surface inhomogeneity, so resonance tracking techniques must be applied[48]. In the case of encapsulated nanowires, the determination of the piezoelectric constants

of nanowires is a complex task, which requires, as well as setting up complex experimental configurations and calibrating the equipment on which the experiment is being performed. It is affected by numerous sources of error derived from the electrostatic interaction between the cantilever and the dielectric surface. But the main aim is to establish the effect of electrical parameters on the piezoelectric properties of the nanowire. For this, PFM could be used as a tool for comparative analysis of the piezoelectric properties with relation to the growth parameters of nanowires. Finally, the polarity orientation of nanowires could be determined from the relative phase between applied AC bias and tip oscillation. For Zn-polarity in ZnO, the vibration induces in-phase oscillations, which is opposite to O-polar polarity generating out-of-phase oscillations.

To capture the vibration of the nanowire through the vibration of the cantilever, it is worthwhile to pay the most careful attention to the invariable position of the laser on the cantilever, since any slightest change in the position of the laser dramatically affects the final result[49]. In this experiment, the same nanowire samples for the electrical characterization were used, i.e., polished nanowires in a dielectric matrix. It should be noted that in this configuration, the nanowires are tightly fixed by the matrix, and only the upper part of the nanowire will be visible in an image of a piezoresponse amplitude. For this reason, we are not able to calculate piezoelectric constant directly because there is no way to measure the absolute value of Δx. Moreover, due to the dielectric matrix, the contribution to the vibration of the nanowire will mainly come from the vertical vibration d_{33} so that we can neglect the lateral d_{31} and d_{15} vibrations. Assuming that all samples of nanowires have the same configuration, we are able to compare the amplitude of the piezoelectric response on nanowires and establish a relationship with different growth parameters. A clear presence of resonance on any point of nanowire indicates the presence of small piezoelectric vibrations that resonate with the flexural vibrations of the cantilever at their resonant frequency in the clamped-pinned mode.[46] The effect of the difference in piezoelectric properties in nanowires was noticeable even at the initial recording of the contact resonance plots. Dual frequency resonance tracking (DFRT) was used exclusively for taking images and finding the zone

of the greatest piezoelectric response on the nanowires. All the series of nanowire samples were measured in the same conditions with the same tip and the same tuning of the laser on the cantilever. At least 20 vibration amplitude images were captured from each sample simultaneously with topography and phase image. As an example, in Figure 4(b) is shown a typical vertical vibration image captured simultaneously with topography in Figure 4(a) and corresponded PFM phase image in Figure 4(c).

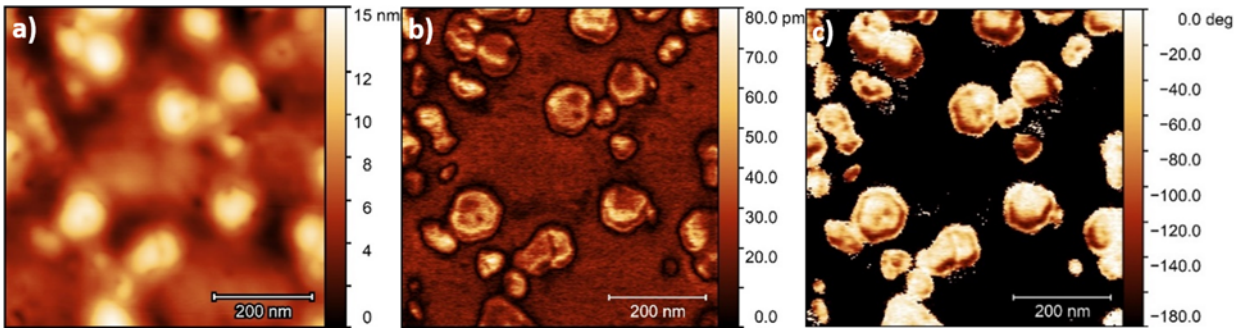

Figure 4. a) Topography of NiD nanowires captured during PFM imaging b) Vertical piezoresponse vibration amplitude image obtained from NiD nanowires, c) Corresponding piezoresponse phase image with a subtracted instrumental phase shift. Scan size – 650 x 650 nm (V_{ac}=400 mV, f_{res}=344kHz, Q_{res} =213, F_{app} = 178nN, k_{EFM} = 4.49 N/m). The examples of images for the whole series of samples are given in supporting information (Figure S2).

It should be clarified that the observed effect is associated exclusively with a change in the electrical field in the nanowire, while the current flow is not necessary in the PFM imaging. Despite the fact that almost all samples showed a fairly high conductivity, at excitation voltages less than 500 mV, due to Schottky barrier, the passing current does not exceed 10 pA and the effects associated with the free charges rearrangement inside the nanowire in response to the applied field[50] can be neglected. Another point should be raised related to the depletion zone created on the point of contact of sample and tip. In fact, adding negative DC bias enhances the contact resonance due to the increase of depletion zone. On the other hand, by applying positive

voltage up to 5V, the contact resonance is reduced but still could be easily detected. In both cases, the comparability of the results did not differ from that shown in Fig. 5, however, for a quantitative analysis of the piezoelectric response, it is necessary to take into account the possible effect of the depletion layer. From the PFM phase image, it can be clearly seen that all nanowires vibrate in phase with a drive voltage, which shows the Zn unipolar nature of the grown nanowires from the seed layers by chemical bath deposition, thereby allowing the difference in piezoelectric vibration coming from the nanowire polarity orientation to be excluded.

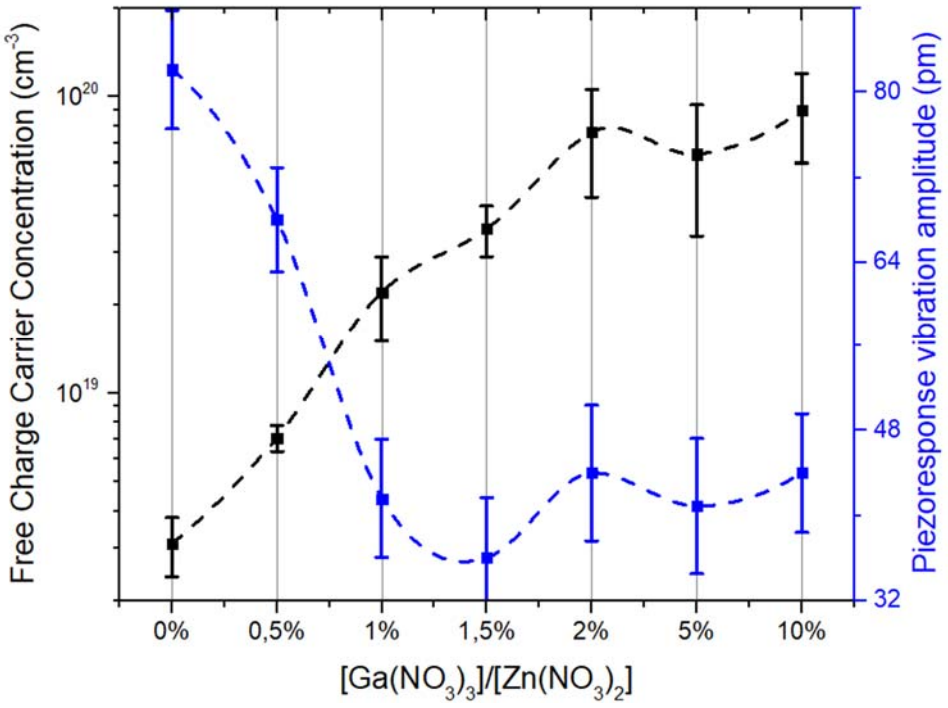

Figure 5. Free charge carrier concentration and amplified piezoresponse amplitude comparison and its relation to differently doped nanowires.

As for vibration images, the variation of the PFM signal on the nanowire has a correlation with the topography – the biggest response is observed in the points, where the angle between the tip and the sample was close to perpendicular. The analysis was performed by two methods: marking image by height threshold and taking the average value of all vibrations that comes from nanowires and statistical comparison of the same diameter nanowires. Both analysis methods showed almost the same result. The results of our studies are shown in Figure 5 in comparison with the

concentration of free charge carriers established using the calibration SSRM method. Residual vibration can be found on the dielectric matrix, most likely caused by electrostatic interaction. However, this vibration was found to be less compared to even the most doped samples, which indicates that the piezoelectric response observed on the nanowire is not parasitic capacitance. Another point that should be mentioned is the possible high impact of electrostatic forces on the PFM measurements[52]. The electrostatic component is usually associated with the contact potential difference V_{cpd}, applied voltages V_{dc}, V_{ac}, and, the most important, a change in the capacitance of the dC/dz in a conventional capacitor between the sample and the probe[53,54]. In our case, the ZnO nanowires exhibit a metallic-type bulk conduction, in which obtaining a significant change in the electrostatic capacitance can be achieved by applying a voltage of more than V_{ac} = 1 V with a less than 5×10^{18} of free charge carrier concentration[25]. When applying the voltage parameters close to the PFM measurements, a change in the electrostatic capacitance was not observed by SCM either on the calibration sample or on the non-doped nanowires (Figures S4, S5 of supporting information).

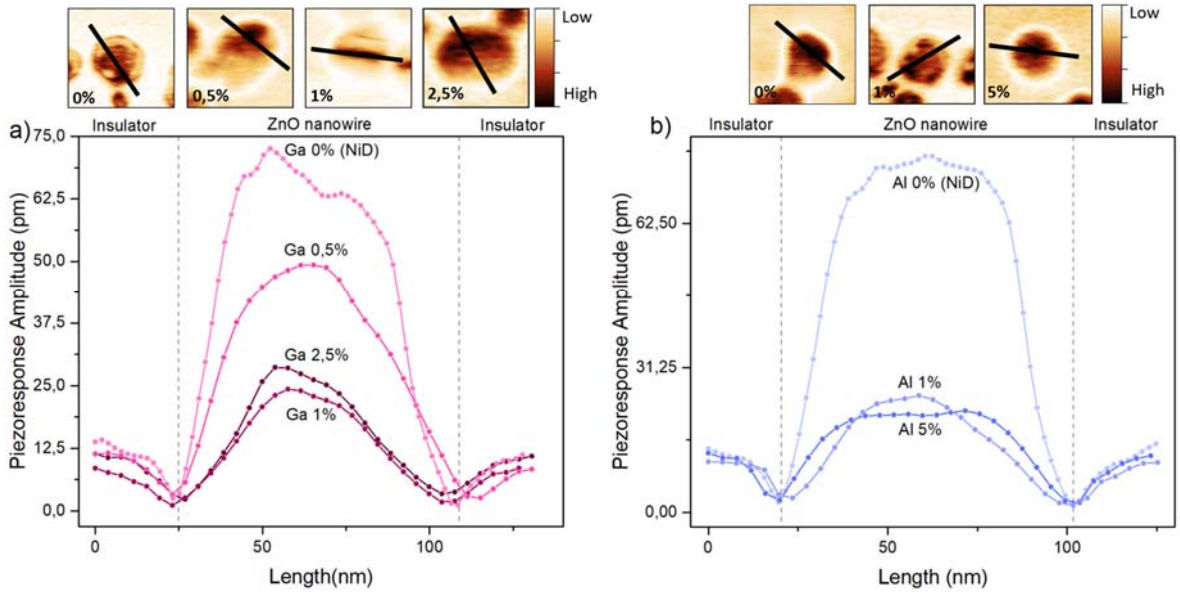

Figure 6. Comparison of piezoresponse amplitude image data profiles taken across the best response area from a) Ga-doped nanowires and b) Al-doped nanowires with a different concentration ratio and with the same diameter equal to 80±5nm.

We observe a significant stable deterioration of the piezoelectric signal with an increase in the free charge carrier concentration and achieve almost twice the degradation of this signal, starting with a $Ga(NO_3)_3$ concentration ratio of 1 % in Ga-doped ZnO nanowires. Further degradation of the PFM signal was not observed even with an increase in the free charge carrier concentration most probably due to large statistical error. Figure 6 shows the vibration amplitude profiles for a) a series of Ga-doped ZnO nanowires and b) a series of Al-doped ZnO nanowires. For both series of samples, an identical behavior was found, namely a drop in the mechanical response by more than twice. Even by assuming that, in Al- and Ga-doped ZnO nanowires, the contribution of mobility and free charge carriers to the conducting properties may differ, their piezoelectric properties remain identical. From the PFM results obtained, it turns out that the piezoelectric properties of nanowires depend on the resistivity as a whole: a separate contribution of the mobility or free charge carriers was not noticed. Conclusively, PFM in DFRT mode is an excellent tool for comparative characterization of the piezoelectric properties of nanostructures since it directly measures the reverse piezoelectric effect and can be used for the more accurate understanding of the effect of free charge carriers on the piezoelectric coefficients.

Discussion

The occurrence of a piezoelectric potential in highly Al- and Ga-doped ZnO nanowires makes a significant contrast to many numerical simulations based on finite element method considering their mechanical, piezoelectric, and semiconducting properties.[10,55,56] These theoretical calculations have reported that the piezoelectric potential in ZnO nanowires should be very low above a critical free charge carrier concentration of around 10^{16}-10^{17} cm^{-3}.[10,55,56] The critical value for the vanishing of the piezoelectric potential is however in strong discrepancy with the widely-reported experimental data in the field of piezoelectric devices made of ZnO nanowires.[57,58] In that field, it has been shown by numerous electrical characterization techniques that ZnO nanowires grown by chemical bath deposition under standard conditions exhibit a high electrical conductivity corresponding to a free charge carrier concentration above 10^{18} cm^{-3},[12,35,59] while exhibiting a

significant piezoelectric potential in the related devices.[57,58] The high free charge carrier concentration has been attributed to the formation of a large number of hydrogen-related defects acting as shallow donors, including interstitial hydrogen and zinc vacancy – hydrogen complexes to name a few.[35] To explore the theoretical calculations with a better refinement, the effects of the surface of ZnO nanowires has recently been considered with care by introducing the surface trap density causing a Fermi level pinning.[7] The prevalence of the surface effects is dependent upon the radius of ZnO nanowires and is strongly improved for typical values below 20 nm as reported by theoretical simulations in the case of the chemical bath deposition method.[60] In the present case, it should be noted that the growth of Al- and Ga-doped ZnO nanowires was achieved at a high pH value, where attractive electrostatic forces favor the incorporation of Al and Ga dopants.[20,21] It is well-known that the growth of ZnO nanowires at a high pH value is responsible for a strong increase in their surface roughness on the *m*-plane sidewalls and in the related density of defects.[20,21,61–63] This has been explained by the strongly anisotropic growth rate favoring the fast elongation of ZnO nanowires as well as by erosion phenomena caused by HO^- ions on their surface. In that sense, the surface trap density in ZnO nanowires grown at a high pH value is expected to be much larger than the typical value of 1-4 10^{13} cm^{-2} obtained in the case of ZnO nanowires grown at a much lower pH value.[64] This certainly accounts for the occurrence of a piezoelectric potential in ZnO nanowires with a free charge carrier concentration exceeding 10^{19} cm^{-3}. Furthermore, the origin of its degradation as the free charge carrier concentration increases most likely comes from the piezoelectric potential screening induced by free electrons as previously observed in nanowire-based pressure sensors[14,55] and theoretically supported by finite element method simulations.[56]

Conclusion

In summary, Al-doped and Ga-doped ZnO nanowires grown by chemical bath deposition with the introduction of $Al(NO_3)_3$ and $Ga(NO_3)_3$ in the bath at a high pH value show a significant increase in their electrical conductivity. The highest concentration of free charge carriers in nanowires was found using the $Ga(NO_3)_3$ concentration ratio of 2% and more and amounted to $(7.6 \pm 3.6) \times 10^{19}$

cm^{-3}. A high concentration of charge free carriers in non-intentionally doped nanowires as compared to ZnO thin films was confirmed, which currently remains at the level of (3.0 ± 3.2) $\times 10^{18}$ cm^{-3}. The gradual Al and Ga doping of nanowires is possible through the more accurate control of the precursor concentration ratio between 0% - 2% for $Ga(NO_3)_3$ and 0% - 1% for $Al(NO_3)_3$. Comparative PFM in DRFT mode have shown the piezoelectric activity of all samples of nanowires, even the most doped ones, which is presumably attributed to the increased surface trap density causing a Fermi level pinning when ZnO nanowires are grown at a high pH value that is favorable for the intentional doping. Moreover, in comparison with the concentration of free charge carriers, a degradation in the piezoelectric response was observed, which experimentally proves the presence of a screening effect in a single ZnO nanowire. Consequently, PFM DFRT can provide valuable information about piezoelectric materials, directly providing the piezoelectric properties and polarity orientation, which are the two most crucial factors impacting the efficiency of the piezoelectric devices.

Experimental Details

Growth and Planarization

Silicon (Si) substrates (2 × 2.5 cm^2) were initially cleaned with acetone and isopropyl alcohol. Subsequently, the ZnO seed layers were deposited by a sol−gel process using dip coating. The solution of chemical precursors was composed of an equimolar mixture of zinc acetate dihydrate and monoethanolamide with a concentration of 375 mM diluted in pure ethanol. To form the sol, the solution was heated and stirred at 60 °C for 12 h and then stirred at room temperature for 12 hours. The samples were then dipped into the solution at room temperature and gently pulled out at a withdrawal speed of 3.3 mm/s under a controlled atmosphere hygrometry smaller than 15%) for the formation of the xerogel film. To evaporate the solvent and residual organic compounds, the samples were annealed at 300 °C for 10 min on a hot plate. The crystallization of the ZnO seed layer was achieved by further annealing at 500 °C for one hour on another hot plate.

ZnO nanowires were formed by chemical bath deposition by putting the samples in a sealed beaker for three hours in an oven kept at 90 °C. The aqueous solution of chemical precursors was composed of zinc nitrate hexahydrate, HMTA, aluminum nitrate nonahydrate, gallium nitrate hydrate[21]. For this study, ZnO nanowires were grown with the same temperature conditions at 85 °C and in an aqueous solution at a high initial pH of 10.9 using a NH_3 concentration of 584 mM with the only variation of $[Al(NO_3)_3]/[Zn(NO_3)_2]$ and $[Ga(NO_3)_3]/[Zn(NO_3)_2]$ ratios from 0 % (NiD) to 10 %. The $Zn(NO_3)_2$ concentration was set to 30 mM. For nanowire samples with a high density, a dip-coating method has been used since the dielectric solution fills the gaps between the nanowires. The dielectric solution was prepared using TEOS (Tetraethyl Orthosilicate), HCl, and ethanol in the proportion of 5 mL, 2 mL, and 37.7 mL. The rate of dipping and pulling out of the sample from the solution was constant and equaled 4 mm/sec. After dipping, the samples soft annealed in air at 100ºC in order to evaporate the liquid. To stabilize the matrix, hard baking was made in an O_2 atmosphere at a temperature of 500 ºC for 30 min. The dip-coating operation was repeated two times on the sample to increase the thickness of the encapsulating matrix. Afterward, chemical-mechanical polishing of the sample carried out using a colloidal silica solution with an average particle size of 25 nm. Polishing time was 8 minutes on a cloth polishing disc. FESEM image of the final result of planarized nanowires has been performed in order to control the final process.

Morphological and chemical properties measurements

The morphology and structural properties of ZnO NWs were measured by top-view and cross-sectional view field emission scanning electron microscopy (FESEM) images using a FEI Quanta 250 field-emission- gun scanning electron microscope. The doping concentrations of Ga layers in MBE grown multilayer sample revealed by secondary ion mass spectroscopy (SIMS) using a CAMECA IMS 7f instrument.

Electric and piezoelectric properties measurements

All the electrical measurements were performed in the ambient conditions of 21 ºC. As an AFM platform, Nanoscope^{tm} Dimension 3100 was used with commercial Electrical mode SSRM and Electrical mode Extended TUNA for capturing I-V curves. A Highly doped conductive diamond tip, CDT-NCHR k = ~40 N/m from Nanosensors^{tm} chosen. The nominal resistance of this tip does not exceed R_{tip} =10 kΩ, which allows neglecting the resistance of the probe since the measured resistance is higher three orders of magnitude. Each sample was measured under identical conditions as the calibration multilayer structure. In all the results for SSRM measurements, the interaction forces were always chosen in such a way as to be sufficient for good contact with the ZnO sample but insufficient for its damage and amounted to $F_{app} = 2,6 \pm 0,4$ μN. I-V measurements between the heavily doped p-type tip and nanowire showed diode behavior, so all measurements were made on the straight part of the barrier, where the linearity of the signal was the most stable. For piezoelectrical measurements, as a lock-in, a HF2LI form Zurich instruments was used in a pair with NT-MDT Ntegra AFM platform. Additional experiments were performed on the Nanoscope^{tm} Dimension 3100 Atomic force microscope, which showed similar results. For measurements, a PPP-EFM tip from Nanosensors^{tm} was used with a nominal value of force constant k = 2.6 N/m and f_{free}=75kHz. The excitation was carried out in the so-called Dual Frequency Resonance Tracking Mode (DFRT), where two excitation frequencies (called “satellite frequencies”) are used on both sides of the contact resonance frequency of the cantilever/tip/sample system. These frequencies were chosen f_{sat}= ±1 kHz away from the resonance frequency.

Acknowledgments

The authors acknowledge the financial support by the French Research National Agency through the project ROLLER (ANR-17-CE09-0033). O. Synhaivskyi would like to thank the financial support of the French Ministry of Universities and Research for his doctoral research grant. P. Gaffuri was supported by a doctoral fellowship from the CDP Eco-SESA project (ANR-15-IDEX-02). The authors further acknowledge the Consortium Lyon Saint-Etienne de Microscopie

(CLYM, FED 4092) for the access to the microscopes. Dr. François JOMARD is acknowledged for performing SIMS measurements.

Associated content

Topography and SSRM resistance images for series of ZnO: Ga samples with doping precursor ranged from 0% to 10% **(Figure S1)**. Piezoresponse amplitude images for series of ZnO: Ga samples with doping precursor ranged from 0% to 5% **(Figure S2)**. Scanning spreading resistance and piezoresponse AFM images for ZnO: Al nanowires sample series **(Figure S3)**. Electrostatic charge variation images (SCM data) captured on calibration ZnO sample and its profiles compared to SIMS depth profile **(Figure S4)**. Topography of ZnO non-doped nanowires and electrostatic charge variation images (SCM data) captured on the same area **(Figure S5)**.

Notes

The authors declare no competing financial interest.

References

(1) Janotti, A.; Van De Walle, C. G. Fundamentals of Zinc Oxide as a Semiconductor. *Reports Prog. Phys.* **2009**, *72* (12). https://doi.org/10.1088/0034-4885/72/12/126501.

(2) Soci, C.; Zhang, A.; Xiang, B.; Dayeh, S. A.; Aplin, D. P. R.; Park, J.; Bao, X. Y.; Lo, Y. H.; Wang, D. ZnO Nanowire UV Photodetectors with High Internal Gain. *Nano Lett.* **2007**, *7* (4), 1003–1009. https://doi.org/10.1021/nl070111x.

(3) Hong, W. K.; Kim, B. J.; Kim, T. W.; Jo, G.; Song, S.; Kwon, S. S.; Yoon, A.; Stach, E. A.; Lee, T. Electrical Properties of ZnO Nanowire Field Effect Transistors by Surface Passivation. *Colloids Surfaces A Physicochem. Eng. Asp.* **2008**, *313–314*, 378–382. https://doi.org/10.1016/j.colsurfa.2007.04.120.

(4) Nguyen, P.; Ng, H. T.; Yamada, T.; Smith, M. K.; Li, J.; Han, J.; Meyyappan,

M. Direct Integration of Metal Oxide Nanowire in Vertical Field-Effect Transistor. *Nano Lett.* **2004**, *4* (4), 651–657. https://doi.org/10.1021/nl0498536.

(5) Wang, Q.; Yang, D.; Qiu, Y.; Zhang, X.; Song, W.; Hu, L. Two-Dimensional ZnO Nanosheets Grown on Flexible ITO-PET Substrate for Self-Powered Energy-Harvesting Nanodevices. *Appl. Phys. Lett.* **2018**, *112* (6). https://doi.org/10.1063/1.5012950.

(6) Lin, Z.; Song, J. Piezoelectric Nanogenerators Based on Zinc Oxide Nanowire Arrays Author(s): Zhong Lin Wang and Jinhui Song Source: *Science (80-.).* **2006**, *312* (5771), 242–246. https://doi.org/10.1126/science.1124005.

(7) Tao, R.; Mouis, M.; Ardila, G. Unveiling the Influence of Surface Fermi Level Pinning on the Piezoelectric Response of Semiconducting Nanowires. *Adv. Electron. Mater.* **2018**, *4* (1), 1–9. https://doi.org/10.1002/aelm.201700299.

(8) Agrawal, R.; Espinosa, H. D. Giant Piezoelectric Size Effects in Zinc Oxide and Gallium Nitride Nanowires. A First Principles Investigation. *Nano Lett.* **2011**, *11* (2), 786–790. https://doi.org/10.1021/nl104004d.

(9) Gao, Y.; Wang, Z. L. Electrostatic Potential in a Bent Piezoelectric Nanowire. The Fundamental Theory of Nanogenerator and Nanopiezotronics. *Nano Lett.* **2007**, *7* (8), 2499–2505. https://doi.org/10.1021/nl071310j.

(10) Hinchet, R.; Lee, S.; Ardila, G.; Montès, L.; Mouis, M.; Wang, Z. L. Performance Optimization of Vertical Nanowire-Based Piezoelectric Nanogenerators. *Adv. Funct. Mater.* **2014**, *24* (7), 971–977. https://doi.org/10.1002/adfm.201302157.

(11) De Luna Bugallo, A.; Donatini, F.; Sartel, C.; Sallet, V.; Pernot, J. Metallic

Core Conduction in Unintentionally Doped ZnO Nanowire. *Appl. Phys. Express* **2015**, *8* (2), 025001. https://doi.org/10.7567/APEX.8.025001.

(12) Cossuet, T.; Donatini, F.; Lord, A. M.; Appert, E.; Pernot, J.; Consonni, V. Polarity-Dependent High Electrical Conductivity of ZnO Nanorods and Its Relation to Hydrogen. *J. Phys. Chem. C* **2018**, *122* (39), 22767–22775. https://doi.org/10.1021/acs.jpcc.8b07388.

(13) Lu, S.; Liao, Q.; Qi, J.; Liu, S.; Liu, Y.; Liang, Q.; Zhang, G.; Zhang, Y. The Enhanced Performance of Piezoelectric Nanogenerator via Suppressing Screening Effect with Au Particles/ZnO Nanoarrays Schottky Junction. *Nano Res.* **2016**, *9* (2), 372–379. https://doi.org/10.1007/s12274-015-0916-6.

(14) Sun, Y.; Yan, X.; Zheng, X.; Li, Y.; Liu, Y.; Shen, Y.; Ding, Y.; Zhang, Y. Effect of Carrier Screening on ZnO-Based Resistive Switching Memory Devices. *Nano Res.* **2017**, *10* (1), 77–86. https://doi.org/10.1007/s12274-016-1267-7.

(15) Scrymgeour, D. A.; Hsu, J. W. P. Correlated Piezoelectric and Electrical Properties in Individual ZnO Nanorods. *Nano Lett.* **2008**, *8* (8), 2204–2209. https://doi.org/10.1021/nl080704n.

(16) Choi, M. Y.; Choi, D.; Jin, M. J.; Kim, I.; Kim, S. H.; Choi, J. Y.; Lee, S. Y.; Kim, J. M.; Kim, S. W. Mechanically Powered Transparent Flexible Charge-Generating Nanodevices with Piezoelectric ZnO Nanorods. *Adv. Mater.* **2009**, *21* (21), 2185–2189. https://doi.org/10.1002/adma.200803605.

(17) Barman, A. Review on Biocompatibility of ZnO Nano Particles. **2015**, 343–352. https://doi.org/10.1007/978-81-322-2256-9_32.

(18) Xu, S.; Wang, Z. L. One-Dimensional ZnO Nanostructures: Solution Growth

and Functional Properties. *Nano Res.* **2011**, *4* (11), 1013–1098. https://doi.org/10.1007/s12274-011-0160-7.

(19) Joo, J.; Chow, B. Y.; Prakash, M.; Boyden, E. S.; Jacobson, J. M. Face-Selective Electrostatic Control of Hydrothermal Zinc Oxide Nanowire Synthesis. *Nat. Mater.* **2011**, *10* (8), 596–601. https://doi.org/10.1038/nmat3069.

(20) Verrier, C.; Appert, E.; Chaix-Pluchery, O.; Rapenne, L.; Rafhay, Q.; Kaminski-Cachopo, A.; Consonni, V. Effects of the PH on the Formation and Doping Mechanisms of ZnO Nanowires Using Aluminum Nitrate and Ammonia. *Inorg. Chem.* **2017**, *56* (21), 13111–13122. https://doi.org/10.1021/acs.inorgchem.7b01916.

(21) Gaffuri, P.; Appert, E.; Chaix-Pluchery, O.; Rapenne, L.; Salaün, M.; Consonni, V. The Path of Gallium from Chemical Bath into ZnO Nanowires: Mechanisms of Formation and Incorporation. *Inorg. Chem.* **2019**, *58* (15), 10269–10279. https://doi.org/10.1021/acs.inorgchem.9b01413.

(22) PAUW, L. J. Van Der. A Method of Measuring the Resistivity and Hall Coefficient on Lamellae of Arbitrary Shape. *Philips Technical Review*. 1958, pp 220–224.

(23) Park, W. Il; Kim, J. S.; Yi, G. C.; Bae, M. H.; Lee, H. J. Fabrication and Electrical Characteristics of High-Performance ZnO Nanorod Field-Effect Transistors. *Appl. Phys. Lett.* **2004**, *85* (21), 5052–5054. https://doi.org/10.1063/1.1821648.

(24) Kim, K.; Kang, H.; Yim, C.; Jeon, D.; Kim, H.; Kim, G.-T.; Lee, J.-S.; Kang, W. Electrical Properties of a Single ZnO Nanowire in a Four-Probe

Configuration. *J. Korean Inst. Electr. Electron. Mater. Eng.* **2005**, *18* (12), 1087–1091. https://doi.org/10.4313/jkem.2005.18.12.1087.

(25) Wang, L.; Guillemin, S.; Chauveau, J. M.; Sallet, V.; Jomard, F.; Brenier, R.; Consonni, V.; Brémond, G. Characterization of Carrier Concentration in ZnO Nanowires by Scanning Capacitance Microscopy. *Phys. Status Solidi Curr. Top. Solid State Phys.* **2016**, *13* (7–9), 576–580. https://doi.org/10.1002/pssc.201510268.

(26) De Wolf, P.; Stephenson, R.; Trenkler, T.; Clarysse, T.; Hantschel, T.; Vandervorst, W. Status and Review of Two-Dimensional Carrier and Dopant Profiling Using Scanning Probe Microscopy. *J. Vac. Sci. Technol. B Microelectron. Nanom. Struct.* **2000**, *18* (1), 361. https://doi.org/10.1116/1.591198.

(27) Zhang, L.; Tanimoto, H.; Adachi, K.; Nishiyama, A. 1-Nm Spatial Resolution in Carrier Profiling of Ultrashallow Junctions By Scanning Spreading Resistance Microscopy. *IEEE Electron Device Lett.* **2008**, *29* (7), 799–801. https://doi.org/10.1109/LED.2008.2000644.

(28) Guillemin, S.; Appert, E.; Roussel, H.; Doisneau, B.; Parize, R.; Boudou, T.; Bremond, G.; Consonni, V. Controlling the Structural Properties of Single Step, Dip Coated ZnO Seed Layers for Growing Perfectly Aligned Nanowire Arrays. *J. Phys. Chem. C* **2015**, *119* (37), 21694–21703. https://doi.org/10.1021/acs.jpcc.5b06180.

(29) Latu-Romain, E.; Gilet, P.; Noel, P.; Garcia, J.; Ferret, P.; Rosina, M.; Feuillet, G.; Lévy, F.; Chelnokov, A. A Generic Approach for Vertical Integration of Nanowires. *Nanotechnology* **2008**, *19* (34). https://doi.org/10.1088/0957-4484/19/34/345304.

(30) Chia, A. C. E.; Lapierre, R. R. Contact Planarization of Ensemble Nanowires. *Nanotechnology* **2011**, *22* (24). https://doi.org/10.1088/0957-4484/22/24/245304.

(31) De Wolf, P. Quantification of Nanospreading Resistance Profiling Data. *J. Vac. Sci. Technol. B Microelectron. Nanom. Struct.* **1998**, *16* (1), 320. https://doi.org/10.1116/1.589804.

(32) Celle, C.; Mouchet, C.; Rouvière, E.; Simonato, J. P.; Mariolle, D.; Chevalier, N.; Brioude, A. Controlled in Situ N-Doping of Silicon Nanowires during VLS Growth and Their Characterization by Scanning Spreading Resistance Microscopy. *J. Phys. Chem. C* **2010**, *114* (2), 760–765. https://doi.org/10.1021/jp9094326.

(33) Wang, L.; Chauveau, J. M.; Brenier, R.; Sallet, V.; Jomard, F.; Sartel, C.; Brémond, G. Access to Residual Carrier Concentration in ZnO Nanowires by Calibrated Scanning Spreading Resistance Microscopy. *Appl. Phys. Lett.* **2016**, *108* (13). https://doi.org/10.1063/1.4945100.

(34) Ko, H. J.; Chen, Y. F.; Hong, S. K.; Wenisch, H.; Yao, T.; Look, D. C. Ga-Doped ZnO Films Grown on GaN Templates by Plasma-Assisted Molecular-Beam Epitaxy. *Appl. Phys. Lett.* **2000**, *77* (23), 3761–3763. https://doi.org/10.1063/1.1331089.

(35) Villafuerte, J.; Donatini, F.; Kioseoglou, J.; Sarigiannidou, E.; Chaix-Pluchery, O.; Pernot, J.; Consonni, V. Zinc Vacancy-Hydrogen Complexes as Major Defects in ZnO Nanowires Grown by Chemical Bath Deposition. *J. Phys. Chem. C* **2020**, *124* (30), 16652–16662. https://doi.org/10.1021/acs.jpcc.0c04264.

(36) Brochen, S.; Lafossas, M.; Robin, I. C.; Ferret, P.; Gemain, F.; Pernot, J.; Feuillet, G. Residual and Intentional N-Type Doping of ZnO Thin Films Grown by Metal-Organic Vapor Phase Epitaxy on Sapphire and ZnO Substrates. *J. Appl. Phys.* **2014**, *115* (11). https://doi.org/10.1063/1.4868591.

(37) Demchenko, D. O.; Earles, B.; Liu, H. Y.; Avrutin, V.; Izyumskaya, N.; Özgür, Ü.; Morkoç, H. Impurity Complexes and Conductivity of Ga-Doped ZnO. *Phys. Rev. B - Condens. Matter Mater. Phys.* **2011**, *84* (7), 1–5. https://doi.org/10.1103/PhysRevB.84.075201.

(38) Ponja, S. D.; Sathasivam, S.; Parkin, I. P.; Carmalt, C. J. Highly Conductive and Transparent Gallium Doped Zinc Oxide Thin Films via Chemical Vapor Deposition. *Sci. Rep.* **2020**, *10* (1), 1–7. https://doi.org/10.1038/s41598-020-57532-7.

(39) Kälblein, D.; Weitz, R. T.; Böttcher, H. J.; Ante, F.; Zschieschang, U.; Kern, K.; Klauk, H. Top-Gate ZnO Nanowire Transistors and Integrated Circuits with Ultrathin Self-Assembled Monolayer Gate Dielectric. *Nano Lett.* **2011**, *11* (12), 5309–5315. https://doi.org/10.1021/nl202767h.

(40) Gabás, M.; Landa-Cánovas, A.; Luis Costa-Krämer, J.; Agulló-Rueda, F.; González-Elipe, A. R.; Díaz-Carrasco, P.; Hernández-Moro, J.; Lorite, I.; Herrero, P.; Castillero, P. et al. Differences in N-Type Doping Efficiency between Al- and Ga-ZnO Films. *J. Appl. Phys.* **2013**, *113* (16). https://doi.org/10.1063/1.4803063.

(41) Güthner, P.; Dransfeld, K. Local Poling of Ferroelectric Polymers by Scanning Force Microscopy. *Appl. Phys. Lett.* **1992**, *61* (9), 1137–1139. https://doi.org/10.1063/1.107693.

(42) Kalinin, S. V.; Morozovska, A. N.; Chen, L. Q.; Rodriguez, B. J. Local Polarization Dynamics in Ferroelectric Materials. *Reports Prog. Phys.* **2010**, *73* (5). https://doi.org/10.1088/0034-4885/73/5/056502.

(43) Gruverman, A. Recent Advances in Functional Testing of Ferroelectric Nanostructures. *Ferroelectrics* **2012**, *433* (1), 88–106. https://doi.org/10.1080/00150193.2012.678145.

(44) Denning, D.; Guyonnet, J.; Rodriguez, B. J. Applications of Piezoresponse Force Microscopy in Materials Research: From Inorganic Ferroelectrics to Biopiezoelectrics and Beyond. *Int. Mater. Rev.* **2016**, *61* (1), 46–70. https://doi.org/10.1179/1743280415Y.0000000013.

(45) Sun, F.; Khassaf, H.; Alpay, S. P. Strain Engineering of Piezoelectric Properties of Strontium Titanate Thin Films. *J. Mater. Sci.* **2014**, *49* (17), 5978–5985. https://doi.org/10.1007/s10853-014-8316-y.

(46) Jesse, S.; Mirman, B.; Kalinin, S. V. Resonance Enhancement in Piezoresponse Force Microscopy: Mapping Electromechanical Activity, Contact Stiffness, and Q Factor. *Appl. Phys. Lett.* **2006**, *89* (2), 11–14. https://doi.org/10.1063/1.2221496.

(47) Rabe, U. Atomic Force Acoustic Microscopy BT - Applied Scanning Probe Methods II: Scanning Probe Microscopy Techniques. *Appl. Scanning Probe Methods* **2006**, *II*, 37–90.

(48) Rodriguez, B. J.; Callahan, C.; Kalinin, S. V.; Proksch, R. Dual-Frequency Resonance-Tracking Atomic Force Microscopy. *Nanotechnology* **2007**, *18* (47). https://doi.org/10.1088/0957-4484/18/47/475504.

(49) Labuda, A.; Proksch, R. Quantitative Measurements of Electromechanical

Response with a Combined Optical Beam and Interferometric Atomic Force Microscope. *Appl. Phys. Lett.* **2015**, *106* (25), 1–5. https://doi.org/10.1063/1.4922210.

(50) Morozovska, A. N.; Svechnikov, S. V.; Eliseev, E. A.; Jesse, S.; Rodriguez, B. J.; Kalinin, S. V. Piezoresponse Force Spectroscopy of Ferroelectric-Semiconductor Materials. *J. Appl. Phys.* **2007**, *102* (11). https://doi.org/10.1063/1.2818370.

(51) Rezeq, M.; Eledlebi, K.; Ismail, M.; Dey, R. K.; Cui, B. Theoretical and Experimental Investigations of Nano-Schottky Contacts. *J. Appl. Phys.* **2016**, *120* (4). https://doi.org/10.1063/1.4959090.

(52) Kim, S.; Seol, D.; Lu, X.; Alexe, M.; Kim, Y. Electrostatic-Free Piezoresponse Force Microscopy. *Sci. Rep.* **2017**, *7* (January), 1–8. https://doi.org/10.1038/srep41657.

(53) Wang, K.; Lu, Y.; Cheng, J.; Zhu, X.; Ji, L. Quantitative Electrostatic Force Measurement and Characterization Based on Oscillation Amplitude Using Atomic Force Microscopy. *AIP Adv.* **2020**, *10* (1). https://doi.org/10.1063/1.5136332.

(54) Balke, N.; Jesse, S.; Yu, P.; Carmichael, B.; Kalinin, S. V.; Tselev, A. Quantification of Surface Displacements and Electromechanical Phenomena via Dynamic Atomic Force Microscopy. *Nanotechnology* **2016**, *27* (42). https://doi.org/10.1088/0957-4484/27/42/425707.

(55) Tian, G.; Xiong, D.; Su, Y.; Yang, T.; Gao, Y.; Yan, C.; Deng, W.; Jin, L.; Zhang, H.; Fan, X. et al. Understanding the Potential Screening Effect through the Discretely Structured ZnO Nanorods Piezo Array. *Nano Lett.* **2020**, *20* (6),

4270–4277. https://doi.org/10.1021/acs.nanolett.0c00793.

(56) Romano, G.; Mantini, G.; Carlo, A. Di; D'Amico, A.; Falconi, C.; Wang, Z. L. Piezoelectric Potential in Vertically Aligned Nanowires for High Output Nanogenerators. *Nanotechnology* **2011**, *22* (46). https://doi.org/10.1088/0957-4484/22/46/465401.

(57) Briscoe, J.; Dunn, S. Piezoelectric Nanogenerators - a Review of Nanostructured Piezoelectric Energy Harvesters. *Nano Energy* **2014**, *14*, 15–29. https://doi.org/10.1016/j.nanoen.2014.11.059.

(58) Consonni, V.; Lord, A. M. Polarity in ZnO Nanowires: A Critical Issue for Piezotronic and Piezoelectric Devices. *Nano Energy* **2021**, *83* (January), 105789. https://doi.org/10.1016/j.nanoen.2021.105789.

(59) Lord, A. M.; Maffeis, T. G.; Walton, A. S.; Kepaptsoglou, D. M.; Ramasse, Q. M.; Ward, M. B.; Köble, J.; Wilks, S. P. Factors That Determine and Limit the Resistivity of High-Quality Individual ZnO Nanowires. *Nanotechnology* **2013**, *24* (43). https://doi.org/10.1088/0957-4484/24/43/435706.

(60) Lopez Garcia, A. J.; Mouis, M.; Consonni, V.; Ardila, G. Dimensional Roadmap for Maximizing the Piezoelectrical Response of ZnO Nanowire-Based Transducers: Impact of Growth Method. *Nanomaterials* **2021**, *11* (4). https://doi.org/10.3390/nano11040941.

(61) Dahiya, A. S.; Boubenia, S.; Franzo, G.; Poulin-Vittrant, G.; Mirabella, S.; Alquier, D. Photoluminescence Study of the Influence of Additive Ammonium Hydroxide in Hydrothermally Grown ZnO Nanowires. *Nanoscale Res. Lett.* **2018**, *13*. https://doi.org/10.1186/s11671-018-2665-4.

(62) Hatch, S. M.; Briscoe, J.; Sapelkin, A.; Gillin, W. P.; Gilchrist, J. B.; Ryan, M.

P.; Heutz, S.; Dunn, S. Influence of Anneal Atmosphere on ZnO-Nanorod Photoluminescent and Morphological Properties with Self-Powered Photodetector Performance. *J. Appl. Phys.* **2013**, *113* (20). https://doi.org/10.1063/1.4805349.

(63) Willander, M.; Yang, L. L.; Wadeasa, A.; Ali, S. U.; Asif, M. H.; Zhao, Q. X.; Nur, O. Zinc Oxide Nanowires: Controlled Low Temperature Growth and Some Electrochemical and Optical Nano-Devices. *J. Mater. Chem.* **2009**, *19* (7), 1006–1018. https://doi.org/10.1039/b816619f.

(64) Zhao, Q. X.; Yang, L. L.; Willander, M.; Sernelius, B. E.; Holtz, P. O. Surface Recombination in ZnO Nanorods Grown by Chemical Bath Deposition. *J. Appl. Phys.* **2008**, *104* (7). https://doi.org/10.1063/1.2991151.

TOC Graphic

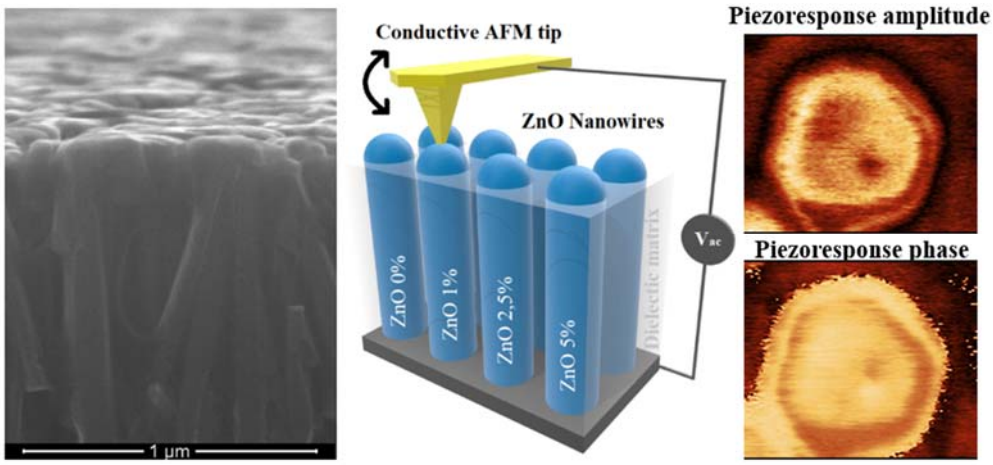
1 µm
Conductive AFM tip
ZnO Nanowires
ZnO 0%
ZnO 1%
ZnO 2,5%
ZnO 5%
Dielectic matrix
V ac
Piezoresponse amplitude
Piezoresponse phase